Zhang *et al.*
*Chinese Journal of Mechanical Engineering* (2022) 35:124
https://doi.org/10.1186/s10033-022-00777-2

Chinese Journal of Mechanical Engineering

ORIGINAL ARTICLE

Open Access

# Design and Analysis of a Novel Compliant Mechanism with RPR Degrees of Freedom

Shuang Zhang[1], Jingfang Liu[1,2*] and Huafeng Ding[1,3]

**Abstract**

A novel compliant mechanism with RPR degrees of freedom (DOF) is proposed where R and P represent rotation and translation DOFs, respectively. The proposed compliant mechanism is obtained from dimension synthesizing a 2-RPU-UPR rigid parallel mechanism with the method of optimization of motion/force transfer characteristic. R, P and U represent rotation, translation and universal pairs, respectively. Firstly, inverse kinematics and Jacobian matrix are analyzed for the dimensional synthesis. Then, output transmission indexes of branches in the parallel mechanism are given. Dimensional synthesis is completed based on the normalized design parameter. And optimization of flexure joints based on constrained energy is carried out. Afterwards, the novel compliant mechanism is obtained by direct replacing method. Mechanical model of the compliant mechanism including static stiffness and input stiffness is built based on the pseudo-rigid body modeling method and virtual work principle. Finally, FEA simulation by Ansys Workbench is carried out to verify DOF, effectiveness of the dimension synthesis, and compliant model. Optimization of motion/force transfer characteristic is first applied for the design of compliant mechanisms to suppress drift of rotation axis in the paper.

**Keywords:** Compliant mechanism, RPR degrees of freedom, Motion/force transfer characteristic, Mechanical model, Optimization

## 1 Introduction

With the excellent characteristics of no backlash, no friction and facilitated manufacture, compliant parallel mechanisms (CPMs) possess potential ability in micro or nano scales precision operations [1–3]. Micro-positioning CPMs with two rotations and one translation (2R1T) are widely applied in the state-of-art precision positioning stages, where orientation of moving platform can be changeable, such as micro-component manufacture and assembly, biological cell manipulation, optical fibers alignment, scanning probe microscopes, and so on [4–9].

The design method of compliant mechanism is always a hot topic in mechanism science. In the past few decades, some effective design methods have been proposed, such as FACT method [10, 11], screw theory method [12] and topological optimization method [13, 14], etc. Flexure hinge-based compliant parallel mechanisms are widely used due to structural similarity to rigid parallel mechanisms, which can be considered as mechanisms in which the rigid joint is replaced by the flexible joint in rigid parallel mechanisms [15–17]. For this reason, direct replacing method [18], which obtains compliant mechanisms by replacing rigid hinges with flexible hinges, is the most popular design method. With the help of existing design methods, a large number of 2R1T compliant mechanisms have been designed for various uses up to now. He et al. [4] presented a novel type compact single mirror laser scanner based on 3-PRS compliant mechanism which is actuated by the permanent magnetic suspension. Kim et al. [5] designed and modeled a precision micro-stage based on the well-known tripod parallel configuration for active micro-vibration control. Park and Lee [6] proposed a piezoelectric-driven tilt mirror for fast laser scanner.

*Correspondence: jfliu@bjut.edu.cn
[1] College of Mechanical Engineering and Applied Electronics Technology, Beijing University of Technology, Beijing 100124, China
Full list of author information is available at the end of the article

Kim et al. [7] developed a nano-precision 2R1T vertical positioning stage which can compensate for the deformation caused by gravity. Lee et al. [8] proposed a 3-DOF out-of-plane nano-positioning stage using a compact bridge-type displacement amplifier. Hao et al. [9] also proposed a 2R1T compliant mechanism based on the constrained-based design method. Most of the existing researches for design of 2R1T compliant mechanism concentrate on designing of one with high natural frequency or with large stroke. However, there are rarely studies on rotational characteristics of 2R1T compliant mechanisms, especially on parasitic motion. The error caused by parasitic motion seriously hinders practical application of the compliant mechanism. It is necessary to eliminate or suppress the parasitic motion of 2R1T compliant mechanisms. According to kinematic characteristics, Li et al. [19] classified 2R1T parallel mechanisms into four categories, which were PU, P*U*, UP and RPR. PU and UP type 2R1T parallel mechanisms possess determined axis of movement and rotation due to constrained chain PU and UP, respectively [20–23]. These two types of parallel mechanisms are not suitable for miniaturization because of its complicated structure due to the additional constraint chains. P*U* type 2R1T parallel mechanisms have two rotation and one translational time-varying axis which are difficult to be acquired [24, 25]. In contrast, RPR type 2R1T parallel mechanisms have two vertical continuous rotation axes relative to the fixed coordinate, which are known. One of them is fixed to the fixed platform; the other one is close to the moving platform, and its position and direction changes in motion [26, 27]. At the same time, this type of mechanisms has relatively simple structure. At present, the existing 2R1T CPMs fall into P*U* type, of which center point of the moving platform could translate not only along $Z$ direction but also along $X$ and $Y$ directions. This phenomenon belongs to parasitic motion. The rotation axis is expected to be as continuous as possible in the working position for facilitate control, especially for micro and nano mechanisms.

In addition, the linear micro-actuation such as piezoelectric actuator is the most popular actuator in CPMs. In the linear elastic deformation problem, axis drift of CPMs with rotation DOF actuated by force mainly lies on the linear deformation caused by actuated force. And the essential function of the mechanism is to transfer the input force and motion to the output to forms desired motion. Motion/force transfer characteristic reflects the essential function [28, 29]. As to rigid parallel mechanisms, motion/force transfer characteristic reflects transfer ability from input motion to output motion, which can be used in singular discrimination. A good motion/force transfer characteristic reflects most of input energy is transferred to desired motion. On the contrary, a bad transfer characteristic reflects that input energy is consumed in the undesired deformation of linkages. Undesired deformation of flexure joints is the main source of parasitic motion. In the paper, optimization based on motion/force transfer characteristic is applied to minimize parasitic motion of an RPR flexure hinge-based compliant mechanism. The RPR compliant mechanism, derived from a 2RPU-UPR rigid parallel mechanism, has good application value in micro-orientation.

The remainder of this paper is organized as follows. Dimension synthesis of the rigid RPR mechanism is carried out in Section 2. Subsequently, the RPR compliant mechanism is obtained by direct replacement and optimization of flexure joints in Section 3. Mechanical model of the compliant mechanism is built based on the pseudo-rigid body model method and virtual work principle in Section 4. In Section 5, validation of DOF, effectiveness of the dimension synthesis and mechanical model by FEA simulation is presented. Finally, conclusions are given.

## 2 Dimension Synthesis of the Rigid RPR Mechanism

The rigid 2-RPU-UPR mechanism [26], selected as the rigid RPR model, is bilaterally symmetrical in initial pose. Its moving and fixed platforms are isosceles right triangles which are parallel to each other, as shown in Figure 1. A fixed frame $o-xyz$ and a moving frame $o'-x'y'z'$ are established at the centers of the fixed and moving platforms, respectively. The axes $x$ and $x'$ point to $A_1$ $B_1$, meanwhile the axes $z$ and $z'$ are perpendicular to the fixed and moving platforms, respectively. In RPU branch, one of the axes of U pair is parallel to that of R pair's, and the other axis is collinear with $x'$ axis. The UPR branch is

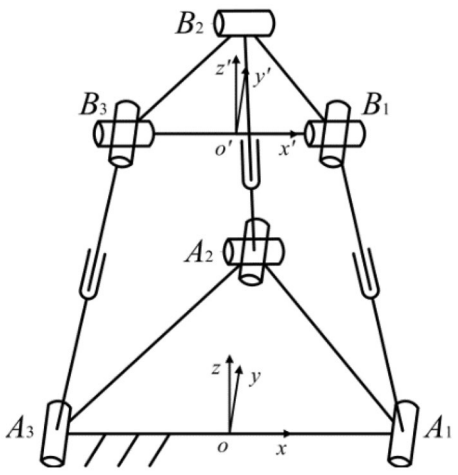


**Figure 1** Sketch of the rigid RPR mechanism

obtained by turning the RPU branch upside down, and its R pair is parallel to $x'$ axis. The DOFs of the mechanism are a rotation around $oA_2$, a translation along $oo'$ and a rotation around $B_1B_3$.

Motion/force transmission characteristic of a mechanism includes two parts: input transmission performance and output transmission performance. The input transmission performance represents the efficiency of power transmitted from the actuated joints to the limbs. While the output transmission performance represents the efficiency of power transmitted from the limbs to the moving platform. The input twist and the transmission wrench of each branch in the RPR mechanism are along the branch in the movement. The input transmission index is equal to cosine of the angle between input twist and transmission wrench. In this case, the input transmission index is always one. Because of its good input transfer characteristics, the rigid mechanism is selected in the paper. And the output transmission index is

$$\eta_i = \frac{\left|\$_{Oi} \circ \$_{Ti}\right|}{\left|\$_{Oi} \circ \$_{Ti}\right|_{\max}}, \tag{1}$$

where $\$_{Oi}$ and $\$_{Ti}$ denotes the output twist and the transmission wrench of the $i$th branch chain, respectively. $\left|\$_{Oi} \circ \$_{Ti}\right|_{\max}$ is presuming efficiency of power, which is referred to Ref. [28]. The output twist and the transmission wrench of branch $A_2B_2$ are a rotation around $A_1B_3$ and a force along $A_2B_2$, respectively. In the initial pose, $A_2B_2$ and $A_1B_3$ are perpendicular to each other. Therefore, the reciprocal product of the output twist and the transmission wrench is the distance between $A_2B_2$ and $A_1B_3$. When the branch $A_2B_2$ is perpendicular to the moving platform, the distance between $A_2B_2$ and $A_1B_3$ reaches the maximum. Furthermore, the output transmission index of branch $A_2B_2$ is equal to 1 when the branch $A_2B_2$ is perpendicular to the moving platform. So only the case that the sizes of moving platform and fixed platform are same is considered in the paper, as thus the output transmission index of branch chain $A_2B_2$ is optimal. The main parameters are shown in Figure 2, where $r_1$ represents distance from the origin of moving coordinate system to the moving pair $B_2$, $r_2$ represents distance from the origin of fixed coordinate system to the moving pair $A_1$, and $P$ represents distance between the origins of two coordinate systems. In the following, inverse kinematic and Jacobian matrix of the 2-RPU-UPR rigid mechanism are analyzed preparing for the dimensional synthesis.

### 2.1 Inverse Kinematics Analysis

Pose of the moving platform can be depicted as

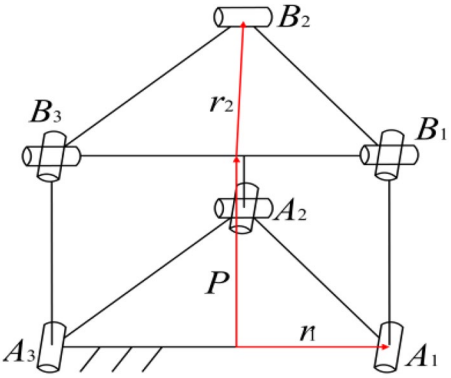


**Figure 2** Schematic of main parameters

$$\boldsymbol{R} = \begin{pmatrix} c\theta & s\theta s\alpha & s\theta c\alpha \\ 0 & c\alpha & -s\alpha \\ -s\theta & c\theta s\alpha & c\theta c\alpha \end{pmatrix}, \tag{2}$$

where $\theta$ and $\alpha$ are the rotation angles of the moving platform around the $y$ axis and $x'$ axis, respectively.

Suppose that the length of $oo'$ is $P$, the coordinate of $o'$ in the fixed frame is $\begin{pmatrix} Ps\theta & 0 & Pc\theta \end{pmatrix}^{\mathrm{T}}$. The coordinates of $B_i$ $(i = 1, 2, 3)$ in the moving frame are

$$\begin{aligned} \boldsymbol{B}_1' &= \begin{pmatrix} r_1 & 0 & 0 \end{pmatrix}^{\mathrm{T}}, \\ \boldsymbol{B}_2' &= \begin{pmatrix} 0 & r_2 & 0 \end{pmatrix}^{\mathrm{T}}, \\ \boldsymbol{B}_3' &= \begin{pmatrix} -r_1 & 0 & 0 \end{pmatrix}^{\mathrm{T}}. \end{aligned} \tag{3}$$

And the coordinates of $B_i$ in the fixed frame can be depicted as

$$\boldsymbol{B}_i = \boldsymbol{R}\boldsymbol{B}_i' + \boldsymbol{oo'}. \tag{4}$$

The coordinates of $A_i$ in the fixed frame can be depicted as

$$\begin{aligned} \boldsymbol{A}_1 &= \begin{pmatrix} r_1 & 0 & 0 \end{pmatrix}^{\mathrm{T}}, \\ \boldsymbol{A}_2 &= \begin{pmatrix} 0 & r_2 & 0 \end{pmatrix}^{\mathrm{T}}, \\ \boldsymbol{A}_3 &= \begin{pmatrix} -r_1 & 0 & 0 \end{pmatrix}^{\mathrm{T}}. \end{aligned} \tag{5}$$

According to the relationship

$$|\boldsymbol{A}_i\boldsymbol{B}_i| = l_i. \tag{6}$$

The inverse kinematics solution of the mechanism can be obtained.

### 2.2 Analysis of Jacobian Matrix

In this section, Jacobian matrix of the rigid RPR mechanism is analyzed based on screw theory. Four subspaces of the 2-RPU-UPR parallel mechanism are obtained by using the method in Ref. [30], and are listed in Appendix.

The velocity of moving platform can be expressed as

$$\boldsymbol{\$}_t \boldsymbol{V} = \boldsymbol{J}_i \dot{\boldsymbol{\theta}}_i,\ (i = 1, 2, 3), \tag{7}$$

where

$$\boldsymbol{\$}_t = \begin{bmatrix} 0 & -c\theta & 0 \\ 1 & 0 & 0 \\ 0 & s\theta & 0 \\ ps\theta & 0 & s\theta \\ 0 & 0 & 0 \\ -pc\theta & 0 & c\theta \end{bmatrix},$$

$$\boldsymbol{V} = \begin{bmatrix} \delta\theta \\ \delta\alpha \\ \delta p \end{bmatrix},$$

$$\boldsymbol{J}_i = \begin{bmatrix} \boldsymbol{J}_{a,i} & \boldsymbol{J}_{c,i} \end{bmatrix},$$

$$\boldsymbol{J}_{c,i} = \begin{bmatrix} \boldsymbol{\$}_{tc,i,1} & \boldsymbol{\$}_{tc,i,2} \end{bmatrix},$$

$$\boldsymbol{J}_{a,i} = \begin{bmatrix} \boldsymbol{\$}_{ta,i,1} & \cdots & \boldsymbol{\$}_{ta,i,4} \end{bmatrix},$$

$$\dot{\boldsymbol{\theta}}_i = \begin{bmatrix} \dot{\boldsymbol{\theta}}_{a,i}^{\mathrm{T}} & \boldsymbol{0}_{2\times1}^{\mathrm{T}} \end{bmatrix}^{\mathrm{T}},$$

$$\dot{\boldsymbol{\theta}}_{a,i} = \begin{bmatrix} \dot{\theta}_{a,i,1} & \dot{\theta}_{a,i,2} & \dot{\theta}_{a,i,2} & \dot{\theta}_{a,i,2} \end{bmatrix}^{\mathrm{T}}.$$

$\boldsymbol{\$}_t$ is motion screw system of the moving platform. $\boldsymbol{V}$ is magnitude of the velocity. $\boldsymbol{J}_i$ is Jacobian matrix of the $i$th branch, $\dot{\boldsymbol{\theta}}_{a,i}$ is the magnitudes of velocities of joints in the branch.

Eq. (8) can be obtained

$$\boldsymbol{J}_i^{-1} \boldsymbol{\$}_t \boldsymbol{V} = \dot{\boldsymbol{\theta}}_i. \tag{8}$$

The following equation is obtained by taking reciprocal product on both sides of Eq. (8) with corresponding actuated wrench

$$\boldsymbol{J}_a \boldsymbol{V} = \boldsymbol{J}_b \dot{\boldsymbol{q}}_a, \tag{9}$$

where

$$\dot{\boldsymbol{q}}_a = \begin{bmatrix} \dot{\boldsymbol{q}}_{a1} & \dot{\boldsymbol{q}}_{a2} & \dot{\boldsymbol{q}}_{a3} \end{bmatrix}^{\mathrm{T}},$$

$$\boldsymbol{J}_a = \begin{bmatrix} \boldsymbol{\$}_{wa,1,2}^{\mathrm{T}} \Delta \boldsymbol{\$}_t \\ \boldsymbol{\$}_{wa,2,3}^{\mathrm{T}} \Delta \boldsymbol{\$}_t \\ \boldsymbol{\$}_{wa,3,2}^{\mathrm{T}} \Delta \boldsymbol{\$}_t \end{bmatrix}_{3\times3},$$

$$\boldsymbol{J}_b = \begin{bmatrix} \boldsymbol{\$}_{wa,1,2}^{\mathrm{T}} \Delta \boldsymbol{\$}_{ta,1,2} & & \\ & \boldsymbol{\$}_{wa,2,3}^{\mathrm{T}} \Delta \boldsymbol{\$}_{ta,2,3} & \\ & & \boldsymbol{\$}_{wa,3,2}^{\mathrm{T}} \Delta \boldsymbol{\$}_{ta,3,2} \end{bmatrix}_{3\times3},$$

$$\Delta = \begin{bmatrix} \boldsymbol{0}_{3\times3} & \boldsymbol{E}_{3\times3} \\ \boldsymbol{E}_{3\times3} & \boldsymbol{0}_{3\times3} \end{bmatrix}.$$

Furthermore, the following equations can be obtained

$$\boldsymbol{J}\boldsymbol{V} = \dot{\boldsymbol{q}}_a, \tag{10}$$

$$\boldsymbol{V} = \boldsymbol{G}\dot{\boldsymbol{q}}_a, \tag{11}$$

where

$$\boldsymbol{J} = \boldsymbol{J}_b^{-1} \boldsymbol{J}_a,$$

$$\boldsymbol{G} = \boldsymbol{J}^{-1}.$$

Substitute Eq. (11) into Eq. (9)

$$\dot{\boldsymbol{\theta}}_i = \boldsymbol{G}_{a,i} \dot{\boldsymbol{q}}_a, \tag{12}$$

where $\boldsymbol{G}_{a,i} = \boldsymbol{J}_i^{-1} \boldsymbol{\$}_t \boldsymbol{G}$.

By combining Eq. (12) of each branch and removing the row vectors corresponding to wrench subspace of actuation and twist subspace of restrictions, the relationship between the velocities of actuators and other kinematics joint is obtained

$$\dot{\boldsymbol{\theta}}_a = \boldsymbol{G}_p \dot{\boldsymbol{q}}_a. \tag{13}$$

### 2.3 Optimization of Motion/Force Transfer Performance

It is also found that the motion/force transfer performance of parallel mechanisms in the initial symmetrical pose is better than that in other pose. And motion range of compliant mechanisms is microscopic. Therefore, the motion/force transfer performance in the initial position is used to evaluate the performance of the RPR mechanism in the paper.

#### *2.3.1 Motion/Force Transmission Analysis*

Due to the symmetrical topological structure in initial position, branch $A_1B_1$ and $A_3B_3$ possess the same output transmission index. Furthermore, the output transmission index of $A_2B_2$ is equal to one. Stated thus, only output transmission index of $A_1B_1$ or $A_3B_3$ needs to be considered. In the paper, the output transmission index of branch $A_1B_1$ is taken into consideration. For convenience, the screw is represented by the row vector in this section.

In initial position, after locking driven joints of $A_2B_2$ and $A_3B_3$, their twist systems are

$$\begin{cases} \left(0\ 1\ 0\ \boldsymbol{oA}_3^{\mathrm{T}} \times (0\ 1\ 0)\right), \\ \left(0\ 1\ 0\ \boldsymbol{oB}_3^{\mathrm{T}} \times \left(0\ 1\ 0\right)\right), \\ \left(1\ 0\ 0\ \boldsymbol{oB}_3^{\mathrm{T}} \times \left(1\ 0\ 0\right)\right), \end{cases} \tag{14}$$

$$\begin{cases} \left(0\ 1\ 0\ \boldsymbol{oA}_2^{\mathrm{T}} \times (0\ 1\ 0)\right), \\ \left(1\ 0\ 0\ \boldsymbol{oA}_2^{\mathrm{T}} \times \left(1\ 0\ 0\right)\right), \\ \left(1\ 0\ 0\ \boldsymbol{oB}_2^{\mathrm{T}} \times \left(1\ 0\ 0\right)\right). \end{cases} \tag{15}$$

And the constrained wrench system can be obtained by taking reciprocal product on the above twist systems

$$\begin{cases} \boldsymbol{H}_1 = \left(0\ 0\ 0\ 0\ 0\ 1\right), \\ \boldsymbol{H}_2 = \left(0\ 1\ 0\ \boldsymbol{oB}_3^{\mathrm{T}} \times \left(0\ 1\ 0\right)\right), \\ \boldsymbol{H}_3 = \left(0\ 0\ 1\ \boldsymbol{oB}_3^{\mathrm{T}} \times \left(0\ 0\ 1\right)\right), \\ \boldsymbol{H}_4 = \left(1\ 0\ 0\ \boldsymbol{oA}_2^{\mathrm{T}} \times \left(1\ 0\ 0\right)\right), \\ \boldsymbol{H}_5 = \left(0\ 0\ 1\ \boldsymbol{oA}_2^{\mathrm{T}} \times \left(0\ 0\ 1\right)\right). \end{cases} \tag{16}$$

The output twist is obtained by solving Eq. (17):

$$\begin{cases} \boldsymbol{\$_O} = \left(\boldsymbol{s}\ \boldsymbol{s}_o\right), \\ \boldsymbol{\$_O} \circ \boldsymbol{H_i} = 0, \\ |\boldsymbol{s}| = 1. \end{cases} \tag{17}$$

The unit transmission wrench of branch chain $A_1B_1$ is

$$\boldsymbol{\$_T} = \left(0\ 0\ 1\ \boldsymbol{oA}_1^{\mathrm{T}} \times \left(0\ 0\ 1\right)\right). \tag{18}$$

The output transmission index can be solved by

$$\eta = \frac{\left|\boldsymbol{\$_T} \circ \boldsymbol{\$_O}\right|}{\left|\boldsymbol{\$_T} \circ \boldsymbol{\$_O}\right|_{\max}}. \tag{19}$$

The presuming efficiency of power $\left|\boldsymbol{\$_T} \circ \boldsymbol{\$_O}\right|_{\max}$ of the RPR mechanism is equal to the distance from $B_1$ to $\boldsymbol{\$}_O$ [28].

#### 2.3.2 Optimization of Design Parameters

In the paper, the RPR mechanism has three design parameters $r_1$, $r_2$ and $P$. And they are normalized as

$$D = \frac{r_1 + r_2 + P}{3}, \tag{20}$$

$$l_1 = \frac{r_1}{D}, \quad l_2 = \frac{r_2}{D}, \quad l_3 = \frac{P}{D}, \tag{21}$$

where $D$ is a normalized factor. $l_1$, $l_2$ and $l_3$ are non-dimensional and normalized parameters.

Considering the actual application, branch lengths and the radius of the platform are not desirable too long or too short. In the paper, the radius of the platform is constrained between one-half to twice the length of the branch. Therefore, the three normalized parameters should satisfy

$$\begin{cases} 0 < l_1, l_2, l_3 < 3, \\ l_1 + l_2 + l_3 = 3, \\ \dfrac{1}{2} l_1 \le l_2 \le 2 l_1. \end{cases} \tag{22}$$

The parameter design space can be depicted as shown in Figure 3. The shaded area shown in Figure 3a is the set of all possible points. For convenience, the reasonable parameter area can be transformed into a triangle plane, as shown in Figure 3b. The relationship between the parameters in spatial space and those in plan space can be depicted as

$$\begin{cases} s = l_2, \\ t = \frac{l_3 - l_1}{\sqrt{3}}. \end{cases} \tag{23}$$

By taking Eqs. (20)–(23) into Eq. (19), the distribution of the output transmission index can be obtained, as shown in Figure 4.

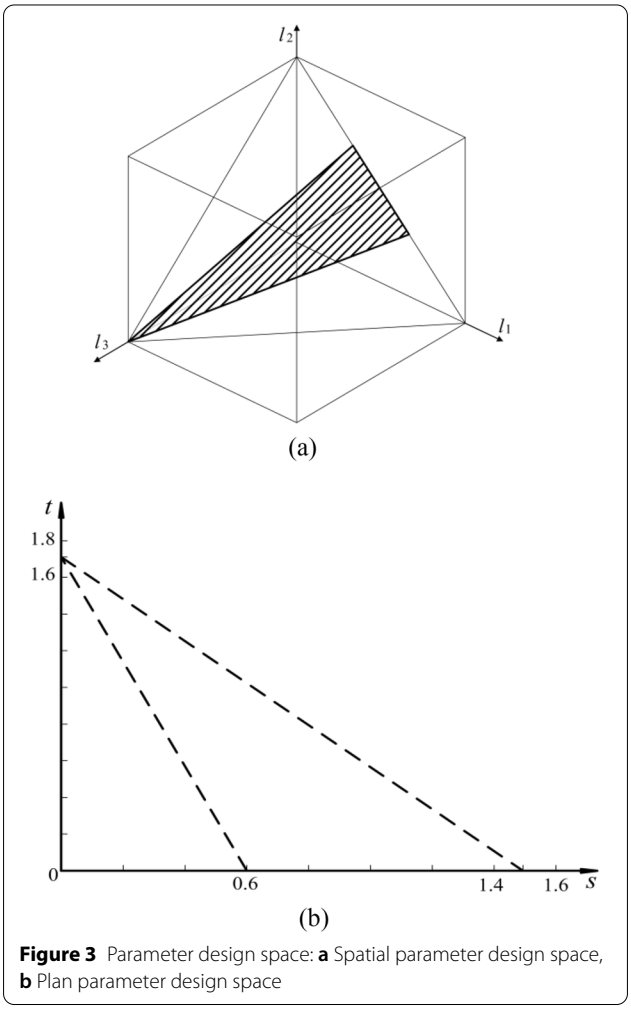


**Figure 3** Parameter design space: **a** Spatial parameter design space, **b** Plan parameter design space

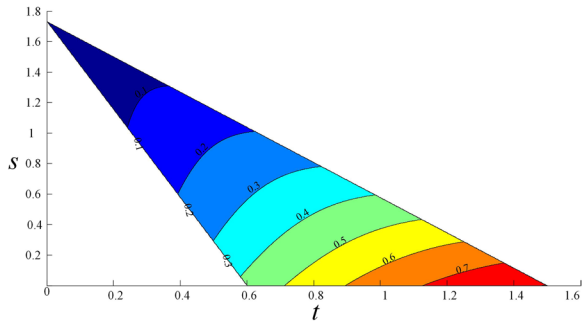


**Figure 4** Distribution of output transmission index

The optimal regions can be found from Figure 4 and it is redly marked. The point

$$\begin{cases} s = 1.5, \\ t = 0, \end{cases} \tag{24}$$

is selected out.

The non-dimensional and normalized parameters are

$$\begin{cases} l_1 = 0.75, \\ l_2 = 1.5, \\ l_3 = 0.75. \end{cases} \tag{25}$$

According to the actual situation and ensure a compact structure consideration, design parameters are determined temporarily.

$$\begin{cases} r_1 = 40 \text{ mm}, \\ r_2 = 80 \text{ mm}, \\ P = 40 \text{ mm}. \end{cases} \tag{26}$$

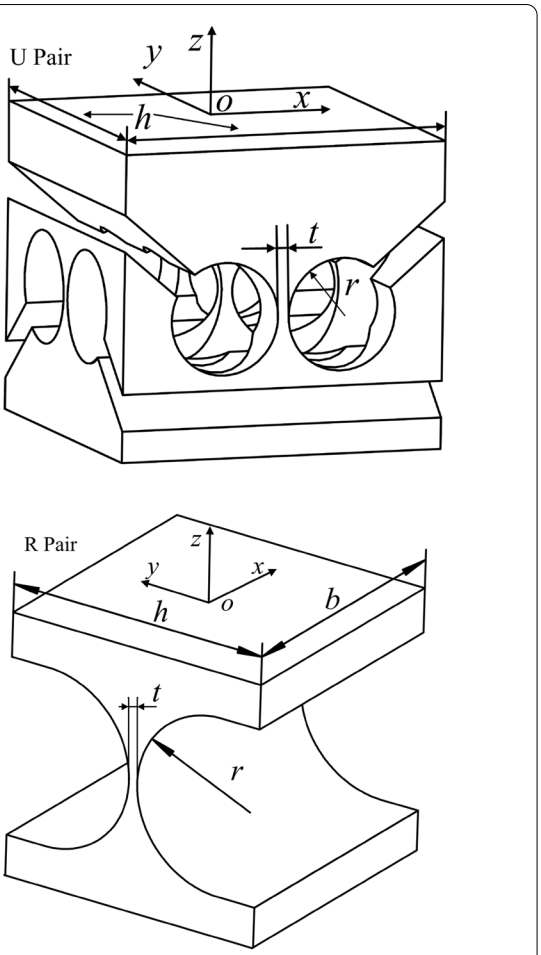


**Figure 5** U compliant joint and R compliant joint

## 3 Design of the Compliant RPR Mechanism

Direct replacing method is used for compliant mechanism in the paper. The core of the method is to replace rigid kinematic pairs in the rigid RPR counterpart with suitable flexible joints. Two kinds of commonly used U compliant joints and R compliant joints are used to replace corresponding rigid kinematics pairs, as shown in Figure 5.

### 3.1 Optimization of Flexible Joints

It is assumed that linkages connecting flexure joints of the RPR compliant mechanism are ideal rigid bodies, and all deformation occurs on flexible joints. Branches of the t mechanism can be regarded as a cantilever beam with one end fixed, the other end subjected to loads applied by moving platform and actuated force. According to statics theory of the rigid parallel mechanism, the load applied by moving platform can be divided into three parts, including constrained wrench, actuated force and another force which makes the major deformation of flexible joints. Undesired motions are constrained by branches. The smaller the deformation of a branch coursed by constrained wrenched is, the better its restraint ability is. Therefore, the optimization of flexible hinge is carried out by taking the sum of the energy, which are caused by unit constrained wrenches, as the objective function. The objective function of the *j*th compliant joint can be defined as

$$\text{Min } f = \sum \boldsymbol{\$}^{c\mathrm{T}} \boldsymbol{C}_j \boldsymbol{\$}^{c}, \tag{27}$$

where $\boldsymbol{C_j}$ is the compliant matrix of the *j*th compliant joint, and $\boldsymbol{\$^c}$ denotes a constrained wrench or an actuated wrench. Using energy as an optimization index can overcome the inconsistency of the dimensionality of translational and rotational compliances.

Flexibility models of the U compliant joint and the R compliant joint are given in Refs. [31] and [32], respectively. In order to remove the coupling between the

force and the moment, the origins of the fixed coordinate systems of the compliant matrices are moved to their structural centers. The matrices of the U compliant joint and the R compliant joint can be expressed as

$$\boldsymbol{C}_U = \begin{pmatrix} cu_{t_x} & & & & & \\ & cu_{ty} & & & & \\ & & cu_{tz} & & & \\ & & & cu_{mx} & & \\ & & & & cu_{my} & \\ & & & & & cu_{mz} \end{pmatrix}, \tag{28}$$

$$\boldsymbol{C}_R = \begin{pmatrix} cr_{t_x} & & & & & \\ & cr_{ty} & & & & \\ & & cr_{tz} & & & \\ & & & cr_{mx} & & \\ & & & & cr_{my} & \\ & & & & & cr_{mz} \end{pmatrix}. \tag{29}$$

After removing the actuated joint, RPU and UPR possess the same structure and constraint wrenches. Therefore, it is only needed to optimize the flexible hinge of any branch in the RPR compliant mechanism.

As to the R joint, the objective function in Eq. (27) can be depicted as

$$\min f = cr_{tx}^2 + cr_{ty}^2 + |\boldsymbol{A}_1\boldsymbol{B}_1|^2 cr_{mx}^2 + cr_{mz}^2. \tag{30}$$

As to the U joint, the objective function in Eq. (27) can be depicted as

$$\min f = cu_{tx}^2 + cu_{ty}^2 + +cu_{mz}^2. \tag{31}$$

Other criteria are used as constraints. The movement range of the end platform is tiny. Normally, when the rotation range of the flexible hinge is relatively large, design demand of the stroke of the compliant mechanism can be fulfilled. Herein, the rotation angle is designed to be more than $\pm 2°$ and the constraint on the rotation angle can be expressed as

$$\theta_{anis,\max} = \frac{r}{Et \cdot SF}\sigma_Y \geq \theta_{des}, \tag{32}$$

where $SF$ is the safety factor, and $\sigma_Y$ is the yield strength.

Manufacturability and volume of the compliant joint are also two important factors. In order to avoid difficulty machining or over size of the compliant joint, the volume is constrained to within 12 mm × 12 mm × 12 mm, and the thinnest part is not less than 0.3 mm. GlobalSearch Function in MATLAB optimization toolbox is used to perform the optimization design. And optimization results are listed in Table 1.

**Table 1** Optimization results of the flexure joints

| R Pair | $r = 4$ mm | $h = 12$ mm | $b = 12$ mm | $t = 0.4$ mm |
|---|---|---|---|---|
| U Pair | $r = 1$ mm | $h = 12$ mm | $t = 0.4$ mm | |

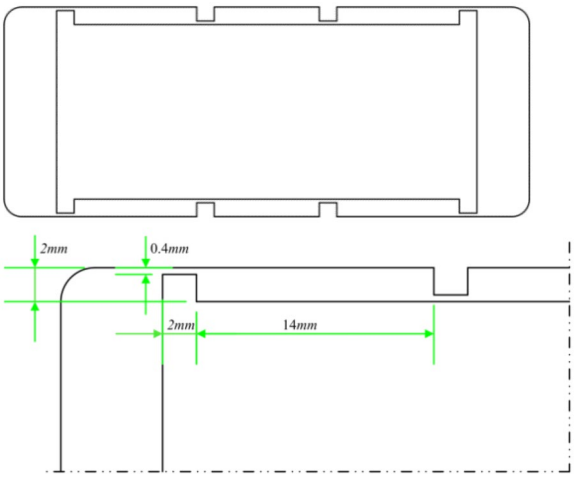


**Figure 6** Sketch of the motion amplifier

### 3.2 Actuated Joint and Motion Amplification Mechanism

The traditional bridge-type amplification mechanism is used as P pair in the paper. According to the overall parameters of the RPR compliant mechanism obtained by dimension synthesis, the structure of the motion amplification mechanism is designed to be as compact as possible, and amplification ratio is about 10. Draw lessons from the design method of the traditional bridge-type amplification mechanism in Refs. [33, 34], and structure of the motion amplifier used in the paper is shown in Figure 6.

The motion amplifier in each branch is placed as closed as to the base in order to relatively low inertia in motion. The structure of the whole RPR compliant mechanism is determined as to now. The simplification ignores the deformations of the leaf spring in other directions. Namely, the displacement amplifier can be regarded as a moving flexible hinge ideally. And sketch of the whole RPR compliant mechanism is shown in Figure 7.

## 4 Mechanical Model of the RPR Compliant Mechanism

The pseudo-rigid body model method and virtual work principle are used to establish statics model of the RPR compliant mechanism. Firstly, the motion amplifier is analyzed. The core of the motion amplifier is the flexible leaf joint. And the leaf joint can be regarded as a pseudo

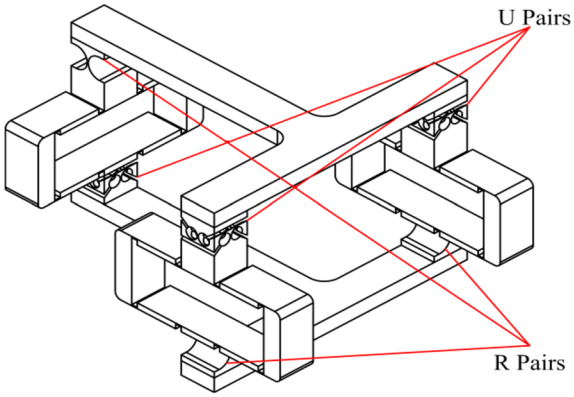


**Figure 7** The obtained RPR compliant mechanism

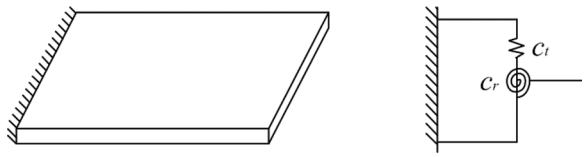


**Figure 8** A flexible leaf joint and its simplified model

rigid body model composed of a rotating pair and a translating pair perpendicular to the flexible leaf, as shown in Figure 8.

In consideration of the force and moment balance at the equilibrium state, the following equation can be obtained

$$f_x l_2 = f_y l_1 + 2m_r, \tag{33}$$

where $l_1$ and $l_2$ are the relative position parameters of the two leaf springs in the displacement amplifier. $l_1 = 0.0016$ m, $l_2 = 0.016$ m.

From the geometric relationship of one quarter of the motion amplifier, we can obtain

$$\begin{cases} d_x = l_2 \Delta\alpha, \\ d_y = l_1 \Delta\alpha - 2\Delta t_1, \end{cases} \tag{34}$$

$$\begin{cases} \Delta\alpha = m_r c_r, \\ \Delta t = f_y c_t. \end{cases} \tag{35}$$

Substitute Eq. (34) and Eq. (35) into Eq. (33), and take the equations of the three branch chains into matrix expressions

$$\begin{cases} \boldsymbol{D}_{in} = \boldsymbol{A}_{11}\boldsymbol{F}_{in} - \boldsymbol{A}_{12}\boldsymbol{F}_{out}, \\ \boldsymbol{D}_{out} = \boldsymbol{A}_{21}\boldsymbol{F}_{in} - \boldsymbol{A}_{22}\boldsymbol{F}_{out}, \end{cases} \tag{36}$$

where

$$\boldsymbol{A}_{11} = \mathrm{diag}\left(\frac{l_2^2 c_r}{4}, \frac{l_2^2 c_r}{4}, \frac{l_2^2 c_r}{4}\right),$$

$$\boldsymbol{A}_{12} = \mathrm{diag}\left(\frac{l_1 l_2 c_r}{4}, \frac{l_1 l_2 c_r}{4}, \frac{l_1 l_2 c_r}{4}\right),$$

$$\boldsymbol{A}_{21} = \mathrm{diag}\left(\frac{l_1 l_2 c_r}{4}, \frac{l_1 l_2 c_r}{4}, \frac{l_1 l_2 c_r}{4}\right),$$

$$\boldsymbol{A}_{22} = \mathrm{diag}\left(\frac{l_1^2 c_r + 4c_t}{4}, \frac{l_1^2 c_r + 4c_t}{4}, \frac{l_1^2 c_r + 4c_t}{4}\right),$$

$$\boldsymbol{F}_{in} = \left(f_{in-1}\ f_{in-2}\ f_{in-3}\right)^{\mathrm{T}},$$

$$\boldsymbol{D}_{in} = \left(d_{in-1}\ d_{in-2}\ d_{in-3}\right)^{\mathrm{T}},$$

$$\boldsymbol{F}_{out} = \left(f_{out-1}\ f_{out-2}\ f_{out-3}\right)^{\mathrm{T}},$$

$$\boldsymbol{D}_{out} = \left(d_{out-1}\ d_{out-2}\ d_{out-3}\right)^{\mathrm{T}}.$$

Secondly, a pseudo-rigid body model is built where motion amplifiers are replaced by three virtual actuated joints with output forces

$$\boldsymbol{F}_{out} = \left(f_{out-1}\ f_{out-2}\ f_{out-3}\right)^{\mathrm{T}}, \tag{37}$$

and output displacement

$$\boldsymbol{D}_{out} = \left(d_{out-1}\ d_{out-2}\ d_{out-3}\right)^{\mathrm{T}}. \tag{38}$$

Apply the virtual work principle to the whole mechanism,

$$\boldsymbol{F}_{out}^{\mathrm{T}} \boldsymbol{D}_{out} = \boldsymbol{D}_J^{\mathrm{T}} \boldsymbol{K}_J \boldsymbol{D}_J, \tag{39}$$

where

$$\boldsymbol{D}_J = \left(\delta\theta_1\ \delta\theta_2\ \cdots\ \delta\theta_9\right),$$

$$\boldsymbol{K}_J = \begin{bmatrix} k_{j1} & & & \\ & k_{j2} & & \\ & & \ddots & \\ & & & k_{j9} \end{bmatrix},$$

$\boldsymbol{K}_J$ is the stiffness matrix, of which diagonal elements are composed the stiffness of major degree of freedom of the passive joint in each branch.

Substitute Eq. (26) into Eq. (39), the relationship between $\boldsymbol{F}_{out}$ and $\boldsymbol{D}_{out}$ can be obtained

$$\boldsymbol{F}_{out} = \boldsymbol{K}'\boldsymbol{D}_{out}, \tag{40}$$

where

$$\boldsymbol{K}' = \boldsymbol{G}_P^{\mathrm{T}}\boldsymbol{K}_J\boldsymbol{G}_P.$$

From Eq. (13), Eq. (36), and Eq. (40), we can obtain

$$\boldsymbol{D} = \boldsymbol{C}\boldsymbol{F}_{in}, \tag{41}$$

$$\boldsymbol{D}_{in} = \boldsymbol{C}_{in}\boldsymbol{F}_{in}, \tag{42}$$

where

$$\boldsymbol{C} = \boldsymbol{G}\left(\boldsymbol{E} + \boldsymbol{A}_{22}\boldsymbol{K}'\right)^{-1}\boldsymbol{A}_{21}, \tag{43}$$

$$\boldsymbol{C}_{in} = \boldsymbol{A}_{11} - \boldsymbol{A}_{12}\boldsymbol{K}'(\boldsymbol{E} + \boldsymbol{A}_{22}\boldsymbol{K}')^{-1}\boldsymbol{A}_{21}, \tag{44}$$

$\boldsymbol{C}$ is the compliant matrix of the whole mechanism. $\boldsymbol{C}_{in}$ is input compliant matrix of the whole mechanism.

## 5 Model Validation with FEA

The DOF, effectiveness of the dimension synthesis, compliant model of the RPR compliant mechanism are verified by FEA with ANSYS Workbench. A 3D virtual model is built which material is assigned as Al-7075 alloy.

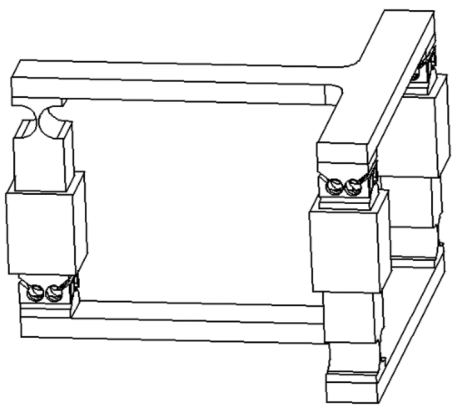

**Figure 9** RPR compliant mechanism for FEA simulation

### 5.1 Validation of DOF and Effectiveness of the Dimension Synthesis

In the section, motion amplifiers are replaced by three rigid translational joint, as shown in Figure 9, in order to avoid undesired deformation of motion amplifiers. When 10 μm is applied to the rigid translational joints, successively, twists of moving platform obtained by theoretical calculation and simulation are listed in Eq. (45) and Eq. (46).

$$T_{th} = \begin{pmatrix} -6.25\times10^{-5} & 12.5\times10^{-5} & -6.25\times10^{-5} \\ -12.5\times10^{-5} & 0 & 12.5\times10^{-5} \\ 0 & 0 & 0 \\ 5.0\times10^{-6} & 0 & -5.0\times10^{-6} \\ 0 & 0 & 0 \\ 5.0\times10^{-6} & 0 & 5.0\times10^{-6} \end{pmatrix}, \tag{45}$$

$$T_{sim} = \begin{pmatrix} -6.24\times10^{-5} & 12.48\times10^{-5} & -6.24\times10^{-5} \\ -12.242\times10^{-5} & 2.32\times10^{-13} & 12.42\times10^{-5} \\ 1.80\times10^{-6} & 3.07\times10^{-8} & 1.83\times10^{-6} \\ 4.6167\times10^{-6} & 2.3994\times10^{-9} & -4.6143\times10^{-6} \\ 2.4357\times10^{-8} & -4.991\times10^{-8} & 2.555\times10^{-8} \\ 4.9924\times10^{-6} & 1.1928\times10^{-8} & 4.9959\times10^{-6} \end{pmatrix}. \tag{46}$$

The first columns in the above matrices are displacement twists of moving platform actuated by $A_1B_1$. The second columns are displacement twists of moving platform actuated by $A_2B_2$. And the third columns are the displacement twists of the moving platform actuated by $A_3B_3$. The matrix obtained by theoretical calculation represented output twists of RPR rigid parallel mechanism. Compare the two matrices, we can find that the matrix obtained by simulation is almost identical to the one obtained by theoretical calculation. Because the compliant mechanism is usually free from or subject to small external forces in practical application, only the situation that end platform is not applied the external force is taken into consideration in the paper. In this case, the degree of freedom of the compliant mechanism can be reflected by the movement of the end platform caused by the actuator. Identity of the matrices shows that the proposed compliant mechanism has desired degree of freedom (RPR DOFs).

Then, two comparative design parameters corresponding to relative bad motion/force transfer performance are selected from Figure 4. And they are used to prove effectiveness of the dimensional synthesis. As same as validation of DOF, motion amplifiers are replaced by three rigid translational joints. And 10 μm is applied to each rigid translational joint, successively. Displacement twists of moving

platform obtained by theoretical calculation and simulation are listed:

$$T_{th-1}=\begin{pmatrix} -12.5\times10^{-5} & 25.0\times10^{-5} & -12.5\times10^{-5} \\ -12.5\times10^{-5} & 0 & 12.5\times10^{-5} \\ 0 & 0 & 0 \\ 5.0\times10^{-6} & 0 & -5.0\times10^{-6} \\ 0 & 0 & 0 \\ 5.0\times10^{-6} & 0 & 5.0\times10^{-6} \end{pmatrix}, \tag{47}$$

$$T_{sim-1}=\begin{pmatrix} -12.46\times10^{-5} & 24.9\times10^{-5} & -12.46\times10^{-5} \\ -12.48\times10^{-5} & 5.05\times10^{-9} & 12.48\times10^{-5} \\ 8.73\times10^{-7} & 1.737\times10^{-8} & -8.90\times10^{-7} \\ 4.8887\times10^{-6} & 5.2534\times10^{-9} & -4.8836\times10^{-6} \\ -5.8996\times10^{-8} & -1.1859\times10^{-7} & -5.9537\times10^{-8} \\ 4.9844\times10^{-6} & 3.0533\times10^{-8} & 4.9853\times10^{-6} \end{pmatrix}, \tag{48}$$

$$T_{th-2}=\begin{pmatrix} -12.5\times10^{-5} & 25.0\times10^{-5} & -12.5\times10^{-5} \\ -6.25\times10^{-5} & 0 & 6.25\times10^{-5} \\ 0 & 0 & 0 \\ -2.5\times10^{-6} & 0 & 2.5\times10^{-6} \\ 0 & 0 & 0 \\ 5.0\times10^{-6} & 0 & 5.0\times10^{-6} \end{pmatrix}, \tag{49}$$

$$T_{sim-2}=\begin{pmatrix} -12.39\times10^{-5} & 24.9\times10^{-5} & -12.39\times10^{-5} \\ -8.32\times10^{-5} & 5.43\times10^{-9} & 8.32\times10^{-5} \\ 2.8\times10^{-7} & -9.78\times10^{-9} & -2.65\times10^{-7} \\ -3.2717\times10^{-6} & -3.1432\times10^{-8} & 3.2702\times10^{-6} \\ -5.6722\times10^{-8} & 1.5078\times10^{-7} & -5.658\times10^{-8} \\ 4.9527\times10^{-6} & 5.9403\times10^{-8} & 4.9529\times10^{-6} \end{pmatrix}. \tag{50}$$

The elements in the matrix obtained by simulation corresponding to the zero elements in the theoretical matrix are extracted

$$\Delta_1=\begin{pmatrix} 0 & 0 & 0 \\ 0 & 2.32\times10^{-13} & 0 \\ 1.80\times10^{-6} & 3.07\times10^{-8} & 1.83\times10^{-6} \\ 0 & 2.3994\times10^{-9} & 0 \\ 2.4357\times10^{-8} & -4.991\times10^{-8} & 2.555\times10^{-8} \\ 0 & 1.1928\times10^{-8} & 0 \end{pmatrix}, \tag{51}$$

$$\Delta_2=\begin{pmatrix} 0 & 0 & 0 \\ 0 & 5.05\times10^{-9} & 0 \\ 8.73\times10^{-7} & 1.737\times10^{-8} & -8.90\times10^{-7} \\ 0 & 5.2534\times10^{-9} & 0 \\ -5.8996\times10^{-8} & -1.1859\times10^{-7} & -5.9537\times10^{-8} \\ 0 & 3.0533\times10^{-8} & 0 \end{pmatrix}, \tag{52}$$

$$\Delta_3=\begin{pmatrix} 0 & 0 & 0 \\ 0 & 5.43\times10^{-9} & 0 \\ 2.8\times10^{-7} & -9.78\times10^{-9} & -2.65\times10^{-7} \\ 0 & -3.1432\times10^{-8} & 0 \\ -5.6722\times10^{-8} & 1.5078\times10^{-7} & -5.658\times10^{-8} \\ 0 & 5.9403\times10^{-8} & 0 \end{pmatrix}. \tag{53}$$

Compare the three matrices in Eqs. (51)–(53), we can find that the linear displacements of the optimized mechanism are smaller than these of the comparison groups. But the angular displacement around $z$-axis of the optimized mechanism is larger than these of the comparison groups. The comparisons indicate that the undesired translations are eliminated, but rotation is not. The dimension synthesis is relatively effective but not perfect. It is insufficiently that only motion/force transfer performance is taken into consideration. In addition to the coupling of force and moment, the main causes of error should include insufficient restraint capacity. The essence of constraint is to resist the deformation of branch in the constraint direction. While optimizing the motion/force transfer performance, the ability of branch constraints should be also considered. The optimization of constraint performance will be studied in our future work.

### 5.2 Validation of the Mechanical Model

A unit force is applied to the two input ends of the three motion amplifiers, successively. The stage deformations along the three working directions are obtained by the FEA simulation. Due to the linear deformation, the elements of compliant matrix of the RPR mechanism are equal to the values of the stage displacements along the working directions. And the stage displacements are given in Eq. (54):

$$T_f = \begin{pmatrix} -1.613 \times 10^{-5} & -7.71 \times 10^{-9} & 1.635 \times 10^{-5} \\ -8.11 \times 10^{-6} & 1.162 \times 10^{-5} & -8.24 \times 10^{-6} \\ 6.6444 \times 10^{-7} & 1.4613 \times 10^{-8} & 6.7338 \times 10^{-7} \end{pmatrix}, \tag{54}$$

$$T_{th-f} = \begin{pmatrix} -1.8704 \times 10^{-5} & 0 & -1.8704 \times 10^{-5} \\ -9.1276 \times 10^{-6} & 1.3255 \times 10^{-5} & -9.1276 \times 10^{-6} \\ 7.4223 \times 10^{-7} & 0 & 7.4223 \times 10^{-7} \end{pmatrix}. \tag{55}$$

The compliant matrix of the RPR mechanism obtained by theoretical calculation is listed in Eq. (55). Comparing Eq. (54) with Eq. (55), the errors between the corresponding elements constitute the following matrix

$$\Delta_2 = \begin{pmatrix} 16.0\% & 0 & 14.4\% \\ 12.5\% & 14\% & 10.8\% \\ 11.7\% & 0 & 10.2\% \end{pmatrix}. \tag{56}$$

From Eq. (56), the compliance model obtained by theoretical calculation is relatively close to the one obtained by the FEA model with most of the errors lower than 16%, which illustrates the theoretical calculation is correct.

Similarly, a unit force is applied to the two input ends of the three motion amplifiers, successively, and deformations of corresponding motion amplifiers are obtained by the FEA simulation. The obtained values of the deformations are equal to elements of the input compliance matrix. The input stiffness matrix obtained by FEA simulation and theoretical calculation are listed in Eq. (57) and Eq. (58), respectively. In addition, the errors between the corresponding elements constitute a matrix, as shown in Eq. (59):

$$C_{in-sim} = \begin{pmatrix} 1.5653 \times 10^{-7} & 0 & 0 \\ 0 & 1.0218 \times 10^{-7} & 0 \\ 0 & 0 & 1.5073 \times 10^{-7} \end{pmatrix}, \tag{57}$$

$$C_{in-th} = \begin{pmatrix} 1.4083 \times 10^{-7} & 0 & 0 \\ 0 & 1.2084 \times 10^{-7} & 0 \\ 0 & 0 & 1.4083 \times 10^{-7} \end{pmatrix}, \tag{58}$$

$$\Delta_3 = \begin{pmatrix} 10.0\% & 0 & 0 \\ 0 & 18.3\% & 0 \\ 0 & 0 & 6.6\% \end{pmatrix}. \tag{59}$$

From Eq. (59), we can find that the maximum margin is 18.3% which is relatively high, but acceptable. The error is mainly caused by undesired deformation of the motion amplifier. The motion amplifier is regarded as planar mechanism which ignores out-of-plane deformation. But it's prone to out-of-plane deformation in application of spatial mechanisms.

$$amp = \begin{pmatrix} 8.4 & 0 & 0 \\ 0 & 9.5 & 0 \\ 0 & 0 & 8.4 \end{pmatrix}. \tag{60}$$

Finally, amplify ratios are obtained by the FEA simulation, and are listed in the following matrix. From Eq. (60), the amplify ratio meets the design requirement which the amplify ratio is equal to about 10.

## 6 Conclusions

The design and analysis of a novel 2R1T compliant mechanism which possesses RPR degree of freedom by direct replacing method are presented in the paper. The moving platform has two rotation axes relative to the fixed coordinate, which are always vertical. One of the two axes is located at the fixed platform; the other is close to the moving platform, and the position and direction both change in motion. Draw on the experience of dimension synthesis method for rigid parallel mechanisms, optimization of motion/force transfer characteristics is applied for design of the RPR compliant mechanism. Based on analysis of kinematic and Jacobian matrix, the optimization index is obtained. Non-dimensional and normalized parameters of the mechanism are used for dimension synthesis. Then, optimization for the compliant joint is carried out and undesired deformations of flexure joints caused by constrained wrenches are minimized. Afterwards, mechanical modeling is built for future application based on the pseudo-rigid body model method and virtual work principle. The DOF, effectiveness of the dimension synthesis, compliant model of the RPR compliant mechanism are verified by FEA simulation. The validation illustrates that the compliant mechanism has RPR degree of freedom. From comparisons of

three design parameter cases, it is found that partial undesired motion is effectively suppressed for the optimal design parameter. The dimension synthesis method used in the paper is applied to the compliant parallel mechanism with rotation degree of freedom which is relatively effective. In the future work, dimension synthesis method for the compliant parallel mechanism with rotation degree of freedom will be improved to reduce parasitic motion.

$$\begin{cases} \$_{wa,1,1} = \left( \boldsymbol{A}_1\boldsymbol{B}_1^{\mathrm{T}} \times \left( 0\ 1\ 0 \right)\ \boldsymbol{o}'\boldsymbol{B}_1^{\mathrm{T}} \times \left( \boldsymbol{A}_1\boldsymbol{B}_1^{\mathrm{T}} \times \left( 0\ 1\ 0 \right) \right) \right)^{\mathrm{T}}, \\ \$_{wa,1,2} = \left( \boldsymbol{A}_1\boldsymbol{B}_1^{\mathrm{T}}\ \boldsymbol{o}'\boldsymbol{A}_1^{\mathrm{T}} \times \boldsymbol{A}_1\boldsymbol{B}_1^{\mathrm{T}} \right)^{\mathrm{T}}, \\ \$_{wa,1,3} = \left( c\theta\ 0\ -s\theta\ \boldsymbol{o}'\boldsymbol{A}_1^{\mathrm{T}} \times \left( c\theta\ 0\ -s\theta \right) \right)^{\mathrm{T}}, \\ \$_{wa,1,4} = \left( 0\ 0\ 0\ c\theta\ 0\ -s\theta \right)^{\mathrm{T}}, \end{cases}$$

## Appendix

In the following screw groups, the number of the subscript indicates its corresponding branch. The bases of the branch permitted twist subspaces:

$$\begin{cases} \$_{ta,1,1} = \left( 0\ 1\ 0\ \boldsymbol{o}'\boldsymbol{A}_1^{\mathrm{T}} \times \left( 0\ 1\ 0 \right) \right)^{\mathrm{T}}, \\ \$_{ta,1,2} = \left( 0\ 0\ 0\ \boldsymbol{A}_1\boldsymbol{B}_1^{\mathrm{T}} \right)^{\mathrm{T}}, \\ \$_{ta,1,3} = \left( 0\ 1\ 0\ \boldsymbol{o}'\boldsymbol{B}_1^{\mathrm{T}} \times \left( 0\ 1\ 0 \right) \right)^{\mathrm{T}}, \\ \$_{ta,1,4} = \left( c\theta\ 0\ -s\theta\ \boldsymbol{o}'\boldsymbol{B}_1^{\mathrm{T}} \times \left( c\theta\ 0\ -s\theta \right) \right)^{\mathrm{T}}, \end{cases}$$

$$\begin{cases} \$_{ta,2,1} = \left( 0\ 1\ 0\ \boldsymbol{o}'\boldsymbol{A}_2^{\mathrm{T}} \times \left( 0\ 1\ 0 \right) \right)^{\mathrm{T}}, \\ \$_{ta,2,2} = \left( c\theta\ 0\ -s\theta\ \boldsymbol{o}'\boldsymbol{A}_2^{\mathrm{T}} \times \left( c\theta\ 0\ -s\theta \right) \right)^{\mathrm{T}}, \\ \$_{ta,2,3} = \left( 0\ 0\ 0\ \boldsymbol{A}_2\boldsymbol{B}_2^{\mathrm{T}} \right)^{\mathrm{T}}, \\ \$_{ta,2,4} = \left( c\theta\ 0\ -s\theta\ \boldsymbol{o}'\boldsymbol{B}_2^{\mathrm{T}} \times \left( c\theta\ 0\ -s\theta \right) \right)^{\mathrm{T}}, \end{cases}$$

$$\begin{cases} \$_{ta,3,1} = \left( 0\ 1\ 0\ \boldsymbol{o}'\boldsymbol{A}_3^{\mathrm{T}} \times \left( 0\ 1\ 0 \right) \right)^{\mathrm{T}}, \\ \$_{ta,3,2} = \left( 0\ 0\ 0\ \boldsymbol{A}_3\boldsymbol{B}_3^{\mathrm{T}} \right)^{\mathrm{T}}, \\ \$_{ta,3,3} = \left( 0\ 1\ 0\ \boldsymbol{o}'\boldsymbol{B}_3^{\mathrm{T}} \times \left( 0\ 1\ 0 \right) \right)^{\mathrm{T}}, \\ \$_{ta,3,4} = \left( c\theta\ 0\ -s\theta\ \boldsymbol{o}'\boldsymbol{B}_3^{\mathrm{T}} \times \left( c\theta\ 0\ -s\theta \right) \right)^{\mathrm{T}}. \end{cases}$$

The bases of the branch constrained wrench subspaces:

$$\begin{cases} \$_{wc,1,1} = \left( 0\ 0\ 0\ \boldsymbol{B}_1\boldsymbol{B}_3^{\mathrm{T}} \times \left( 0\ 1\ 0 \right)^{\mathrm{T}} \right)^{\mathrm{T}}, \\ \$_{wc,1,2} = \left( 0\ 1\ 0\ \boldsymbol{o}'\boldsymbol{B}_1^{\mathrm{T}} \times \left( 0\ 1\ 0 \right) \right)^{\mathrm{T}}, \end{cases}$$

$$\begin{cases} \$_{wc,2,1} = \left( 0\ 0\ 0\ -s\theta\ 0\ -c\theta \right)^{\mathrm{T}}, \\ \$_{wc,2,2} = \left( c\theta\ 0\ -s\theta\ \boldsymbol{o}'\boldsymbol{A}_2^{\mathrm{T}} \times \left( c\theta\ 0\ -s\theta \right) \right)^{\mathrm{T}}, \end{cases}$$

$$\begin{cases} \$_{wc,3,1} = \left( 0\ 0\ 0\ \boldsymbol{B}_1\boldsymbol{B}_3^{\mathrm{T}} \times \left( 0\ 1\ 0 \right)^{\mathrm{T}} \right)^{\mathrm{T}}, \\ \$_{wc,3,2} = \left( 0\ 1\ 0\ \boldsymbol{o}'\boldsymbol{B}_3^{\mathrm{T}} \times \left( 0\ 1\ 0 \right) \right)^{\mathrm{T}}. \end{cases}$$

The bases of the branch actuated wrench subspaces:

$$\begin{cases} \$_{wa,2,1} = \left( 0\ 0\ 0\ 0\ 1\ 0 \right)^{\mathrm{T}}, \\ \$_{wa,2,2} = \left( 0\ 1\ 0\ \boldsymbol{o}'\boldsymbol{B}_2^{\mathrm{T}} \times \left( 0\ 1\ 0 \right) \right)^{\mathrm{T}}, \\ \$_{wa,2,3} = \left( \boldsymbol{A}_2\boldsymbol{B}_2^{\mathrm{T}}\ \boldsymbol{o}'\boldsymbol{A}_2^{\mathrm{T}} \times \boldsymbol{A}_2\boldsymbol{B}_2^{\mathrm{T}} \right)^{\mathrm{T}}, \\ \$_{wa,2,4} = \left( 0\ 1\ 0\ \boldsymbol{o}'\boldsymbol{A}_2^{\mathrm{T}} \times \left( 0\ 1\ 0 \right) \right)^{\mathrm{T}}, \end{cases}$$

$$\begin{cases} \$_{wa,3,1} = \left( \boldsymbol{A}_3\boldsymbol{B}_3^{\mathrm{T}} \times (\ 0\ 1\ 0\ )\ \boldsymbol{o}'\boldsymbol{B}_3^{\mathrm{T}} \times \left( \boldsymbol{A}_3\boldsymbol{B}_3^{\mathrm{T}} \times \left( 0\ 1\ 0 \right) \right) \right)^{\mathrm{T}}, \\ \$_{wa,3,2} = \left( \boldsymbol{A}_3\boldsymbol{B}_3^{\mathrm{T}}\ \boldsymbol{o}'\boldsymbol{A}_3^{\mathrm{T}} \times \boldsymbol{A}_3\boldsymbol{B}_3^{\mathrm{T}} \right)^{\mathrm{T}}, \\ \$_{wa,3,3} = \left( c\theta\ 0\ -s\theta\ \boldsymbol{o}'\boldsymbol{A}_3^{\mathrm{T}} \times \left( c\theta\ 0\ -s\theta \right) \right)^{\mathrm{T}}, \\ \$_{wa,3,4} = \left( 0\ 0\ 0\ c\theta\ 0\ -s\theta \right)^{\mathrm{T}}. \end{cases}$$

The bases of the branch constrained twist subspaces:

$$\begin{cases} \$_{tc,1,1} = \left( \boldsymbol{A}_1\boldsymbol{B}_1^{\mathrm{T}}\ \boldsymbol{o}'\boldsymbol{B}_1^{\mathrm{T}} \times \boldsymbol{A}_1\boldsymbol{B}_1^{\mathrm{T}} \right)^{\mathrm{T}}, \\ \$_{tc,1,2} = \left( 0\ 0\ 0\ 0\ 1\ 0 \right)^{\mathrm{T}}, \end{cases}$$

$$\begin{cases} \$_{tc,2,1} = \left( \boldsymbol{A}_2\boldsymbol{B}_2^{\mathrm{T}}\ \boldsymbol{o}'\boldsymbol{A}_2^{\mathrm{T}} \times \boldsymbol{A}_2\boldsymbol{B}_2^{\mathrm{T}} \right)^{\mathrm{T}}, \\ \$_{tc,2,2} = \left( 0\ 0\ 0\ c\theta\ 0\ -s\theta \right)^{\mathrm{T}}, \end{cases}$$

$$\begin{cases} \$_{tc,3,1} = \left( \boldsymbol{A}_3\boldsymbol{B}_3^{\mathrm{T}}\ \boldsymbol{o}'\boldsymbol{B}_3^{\mathrm{T}} \times \boldsymbol{A}_3\boldsymbol{B}_3^{\mathrm{T}} \right)^{\mathrm{T}}, \\ \$_{tc,3,2} = \left( 0\ 0\ 0\ 0\ 1\ 0 \right)^{\mathrm{T}}. \end{cases}$$

**Acknowledgements**
Not applicable.

**Authors' contributions**
SZ is responsible for the main content of the manuscript, including theoretical analysis and calculation, as well as writing, JL was in charge of the whole trial, HD assisted with theoretical analysis and manuscript revision. All authors read and approved the final manuscript.

**Authors' Information**
Shuang Zhang, born in 1991, is currently a PhD candidate in mechanical engineering at *Beijing University of Technology, China*. He received his bachelor degree from *Beijing University of Technology, China*, in 2017. His research interests include compliant mechanisms, and parallel mechanisms.
Jingfang Liu, born in 1985, is currently an associate professor at *Beijing University of Technology, China*. She received her doctor degree in mechanical engineering from *Yanshan University, China*, in 2011.
Huafeng Ding, born in 1977, is currently a professor at *Beijing University of Technology, China*. He received the first Ph.D. degrees in mechanical engineering from *Yanshan University, China*, in 2007, and the second Ph.D. degree in mechanical engineering from the *University of Duisburg-Essen, Germany*, in 2015.

**Funding**
Supported by National Natural Science Foundation of China (Grant No. 51975007).

**Competing Interests**
The authors declare no competing financial interests.

**Author Details**
[1]College of Mechanical Engineering and Applied Electronics Technology, Beijing University of Technology, Beijing 100124, China. [2]Key Laboratory of Advanced Manufacturing Technology, Beijing University of Technology, Beijing 100124, China. [3]School of Mechanical Engineering and Electronic Information, China University of Geosciences (Wuhan), Wuhan 430074, China.

Received: 1 July 2020 Revised: 5 March 2021 Accepted: 6 July 2022
Published online: 12 October 2022

**References**
[1] B J Yi, G Chung, H Na, et al. Design and experiment of a 3-DOF parallel micro-mechanism utilizing flexure hinges. *IEEE Transaction on Robotics and Automation*, 2003, 19(4): 604-612.
[2] C Werner, P Rosielle, M Steinbuch. Design of a long stroke translation stage for AFM. *International Journal of Machine Tools & Manufacture*, 2010, 50(2):183-190.
[3] K B Choi, D H Kim. Monolithic parallel linear compliant mechanism for two axes ultra-precision linear motion. *The Review of Scientific Instruments*, 2006,77(6): 065106-1-065106-7.
[4] N He, W Jia, M Gong, et al. Design and mechanism analysis of a novel type compact single mirror laser scanner. *Sensors and Actuators A-Physical*, 2006, 125(2): 482-485.
[5] H S Kim, Y M Cho. Design and modeling of a novel 3-DOF precision micro-stage. *Mechatronics*, 2009, 19(5): 598-608.
[6] J H Park, H S Lee. Design of a piezoelectric-driven tilt mirror for a fast laser scanner. *Japanese Journal of Applied Physics*, 2012, 51(9): 1-14.
[7] H Kim, J Kim, D Ahn, et al. Development of a nano-precision 3-DOF vertical positioning system with a flexure hinge. *IEEE Transactions on Nanotechnology*, 2013, 12(2): 234-245.
[8] H J Lee, H C Kim, H Y Kim, et al. Optimal design and experiment of a three-axis out-of-plane nano positioning stage using a new compact bridge-type displacement amplifier. *The Review of Scientific Instruments*, 2013, 84(11): 115103.
[9] G B Hao, X He. Designing a monolithic tip-tilt-piston flexure manipulator. *Archives of Civil & Mechanical Engineering*, 2017, 17(4): 871-879
[10] J B Hopkins, M L Culpepper. Synthesis of multi-degree of freedom parallel flexure system concepts via Freedom and Constraint Topology (FACT)—Part I: Principles. *Precision Engineering*, 2010, 34(2): 259-270.
[11] J B Hopkins, M L Culpepper. Synthesis of multi-degree of freedom parallel flexure system concepts via Freedom and Constraint Topology (FACT)—Part II: Practice. *Precision Engineering*, 2010, 34(2): 271-278.
[12] J Yu, S Li, H J Su, et al. Screw theory based methodology for the deterministic type synthesis of flexure mechanisms. *Journal of Mechanisms and Robotics*, 2011, 3(3): 031008.
[13] G Ananthasuresh, S Kota, Y Gianchandani. A methodical approach to the design of compliant micro mechanisms. *Solid-state Sensor and Actuator Workshop, Hilton Head Island, SC*, 1994: 189-192.
[14] M Jin, X Zhang. A new topology optimization method for planar compliant parallel mechanisms. *Mechanism and Machine Theory*, 2016, 9(5): 42-58.
[15] Y K Yong, T F Lu. Kinetostatic modeling of 3-RRR compliant micro-motion stages with flexure hinges. *Mechanism and Machine Theory*, 2009, 44(6): 1156-1175.
[16] Y Li, Q Xu. A totally decoupled piezo-driven XYZ flexure parallel micropositioning stage for micro/nanomanipulation. *IEEE Transactions on Automation science and Engineering*, 2011, 8(2): 265-279.
[17] Y Li, Q Xu. Design and optimization of an XYZ parallel micromanipulator with flexure hinges. *Journal of Intelligent and Robotic Systems*, 2009, 55(4): 77-402.
[18] Z Gao, D Zhang. Design, analysis and fabrication of a multidimensional acceleration sensor based on fully decoupled compliant parallel mechanism. *Sensors and Actuators A-Physical*, 2010, 163(1): 418-427.
[19] Q C Li, X X Chai, Q H Chen. Review on 2R1T 3-DOF parallel mechanisms. *Chinese Science Bulletin*, 2017, 62(14): 1507-1519.
[20] F Xie, X J Liu, J Wang. A 3-DOF parallel manufacturing module and its kinematic optimization. *Robotics and Computer Integrated Manufacturing*, 2012, 2(8): 334-343.
[21] F Xie, X J Liu, Li T. A comparison study on the orientation capability and parasitic motions of two novel articulated tool heads with parallel kinematics. *Advances in Mechanical Engineering*, 2013, 5: 249103.
[22] X Kong, C M Gosselin. Type synthesis of three-DOF up-equivalent parallel manipulators using a virtual-chain approach. *Advances in Robot Kinematics,* Netherlands: Springer, 2006: 123-132.
[23] T Huang, M Li, X Zhao, et al. Conceptual design and dimensional synthesis for a 3-DOF module of the TriVariant-a novel 5-DOF reconfigurable hybrid robot. *IEEE Transactions on Robotics*, 2005, 2(1): 449-456.
[24] K H Hunt. Structural kinematics of in-parallel-actuated robot-arms. *Journal of Mechanical Design*, 1983, 105: 705-712.
[25] T Huang, H Liu. *Parallel mechanism having two rotational and one translational degrees of freedom.* Patent 7793564, USA 2010.
[26] Q C Li, Q H Chen, et al. *Three degree of freedom parallel mechanism with two vertical staggered axes.* Patent, CN202292114U, China 2010.
[27] Q C Li, J M Hervé. Type synthesis of 3-DOF RPR-equivalent parallel mechanisms. *IEEE Transaction on Robotics*, 2014, 30: 1333-1343.
[28] J Wang, C Wu, X J Liu. Performance evaluation of parallel manipulators: Motion/force transmissibility and its index. *Mechanism and Machine Theory*, 2010, 45(10): 1462-1476.
[29] X J Liu, J Wang. A new methodology for optimal kinematic design of parallel mechanisms. *Mechanism and Machine Theory*, 2007, 42(9): 1210-1224.
[30] T Huang, H T Liu, D G Chetwynd. Generalized Jacobian analysis of lower mobility manipulators. *Mechanism and Machine Theory*, 2011, 46(5): 831-844.
[31] G Palmieri, M C Palpacelli, M Callegari. Study of a fully compliant U-joint designed for minirobotics applications. *Journal of Mechanical Design*, 2012, 134(12): 1-9.
[32] G Chen, X Liu, Y Du. Elliptical-arc-fillet flexure hinges: toward a generalized model for commonly used flexure hinges. *Journal of Mechanical Design*, 2011, 133(8): 081002.
[33] P B Liu, P Yan. A new model analysis approach for bridge-type amplifiers supporting nano-stage design. *Mechanism and Machine Theory*, 2016, 99(5): 176-188.
[34] K Qian, Y Xiang, C Fang, et al. Analysis of the displacement amplification ratio of bridge-type mechanism. *Mechanism and Machine Theory*, 2015, 87(5): 45-56.